Journal of Civil Structural Health Monitoring
https://doi.org/10.1007/s13349-024-00817-6

ORIGINAL PAPER

Computer vision-based dynamic identification of a reinforced concrete elevated water tank

Stefano De Santis[1] · Marialuigia Sangirardi[1,2] · Vittorio Altomare[1] · Pietro Meriggi[1] · Gianmarco de Felice[1]

Received: 9 January 2024 / Accepted: 29 May 2024

Abstract
There is a growing need for monitoring the structural health conditions of aging structures and for prioritizing maintenance works to extend their safe service life. This requires cheap, flexible, and reliable tools suitable for everyday use in engineering practice. This paper presents a computer vision-based technique combining motion magnification and statistical algorithms to calculate structural natural frequencies under environmental noise excitation, and its application to a reinforced concrete elevated water tank. Digital videos were recorded from various standpoints and post-processed by tracking in time either the variation of the grey-intensity or the motion of selected pixels. Computer vision-based outcomes were validated against accelerometric measurements and integrated to them to improve the understanding of the dynamic behaviour of the water tower, which, counterintuitively, resulted anything but trivial to predict.

Keywords Dynamic identification · Motion magnification · Principal component analysis · Target tracking · Field monitoring · Digital survey · Operational modal analysis

1 Introduction

Managing the aging building stock primarily needs effective and cost-efficient strategies to ensure safety, rank maintenance works, and preserve heritage structures during time. Material deterioration, damage development, and increasing loading demands make periodic condition assessment undeniable and, to this aim, the role of structural health monitoring (SHM) tools is continuously growing [1].

✉ Stefano De Santis
stefano.desantis@uniroma3.it

✉ Marialuigia Sangirardi
marialuigia.sangirardi@eng.ox.ac.uk

Vittorio Altomare
vittorio.altomare@uniroma3.it

Pietro Meriggi
pietro.meriggi@uniroma3.it

Gianmarco de Felice
gianmarco.defelice@uniroma3.it

[1] Department of Civil, Computer and Aeronautical Engineering, Roma Tre University, Via Vito Volterra 62, 00146 Rome, Italy

[2] Department of Engineering Science, University of Oxford, Oxford OX1 3PJ, UK

One of the most adopted approaches for detecting global modifications of structural behaviour is based on the analysis of vibration test data. A decrease of the fundamental frequency and a modification of modal shapes, which are usually calculated from acceleration (or velocity) time histories, can be associated with structural damage [2]. Even though sensor location optimization allows reducing the number of accelerometers (or velocimeters) [3], using devices that are physiclly fixed to the structure entails inherent drawbacks, such as purchase costs, installation and maintenance efforts, possible damage to instrumentation, and need of cabling for power supply and data transmission (wireless sensors are nowadays available but these are more expensive than traditional ones). For these reasons, data are generally recorded only at a limited number of locations, selected a priori with engineering judgement.

In fact, what above constitutes a strong constraint, which can be partly overcome by contactless monitoring, whose development in recent years has been triggered by the rapid advancement of optical tools and computer vision post-processing techniques [4–13]. Such methods have been reliably applied in various contexts, providing displacement time histories, from which modal parameters are extracted in a cheaper and faster process, if compared to standard accelerometric acquisitions. When ambient noise (traffic or wind)

Published online: 20 July 2024

induced vibrations are concerned, optical tools might fail to recognize structural displacements, due to their subtle entity. To cope with this, motion magnification algorithms are a necessary pre-processing step. They amplify displacements within a pre-determined frequency range with a desired magnification factor and have been successfully included in the framework of visual-based SHM applications [14–18]. Architectural heritage buildings are well suited for the application of computer-vision-based techniques for dynamic identification under environmental noise. On one hand, they particularly benefit from periodic SHM and, on the other hand, require non-invasive inspection methods. Within the wide panorama of the valuable building stock, elevated water tanks are not rarely considered as a landmark in urban and more rural contexts and have captured growing attention in engineering research and practice. Nowadays they tend to be considered industrial-heritage assets for their technological, historical, social, and esthetical value. At the same time, their structural weakness, mainly due to material deterioration and seismic vulnerability, makes effective and cost-efficient SHM methods mostly required for their periodic assessment.

In this work, a computer vision-based method was applied for the dynamic identification of a reinforced concrete elevated water tank. The structure was inspected through digital survey and non-destructive field tests (§3). Its dynamic properties were preliminary assessed through simplified analytical and numerical methods (§4) and then detected through monitoring with accelerometers (§5). The computer vision-based method provided the fundamental frequencies from digital videos, which were post-processed by a phase-based motion magnification and a principal component analysis. Either the motion of pixels or their intensity variation was tracked (§6.1), following a methodology recently validated both in small scale laboratory tests [19] and in large scale shake table tests [20]. Computer vision-based outcomes were validated against those provided by accelerometers and conveniently integrated information to gain an improved understanding of the dynamic properties of the structure (§6.2).

2 Structural features of elevated water tanks and scientific background

2.1 Architectural significance

Elevated water tanks, also known as water towers, are a typical element of city landscapes. They have been built since the XVIII Century in the vicinity of rail stations for supplying water to the railway transport system, when steam locomotives were in use, and to industrial areas, where water was needed in manufacturing processes. They are now considered industrial-heritage assets and listed as architectural heritage for their technological, historical, social, and esthetical value. Some of them are rated as UNESCO monuments, as remaining symbols of the industrial culture in urban areas [21].

The first water towers were built in masonry, whereas reinforced concrete (RC) became predominant since 1940s. Differently from industrial tanks storing oils and liquified gasses, which are usually ground supported and squat, water tanks are often elevated to ensure proper hydraulic head, resulting in tall and slender structures. The tank is supported either by a shaft structure or a frame and may be encased in a masonry building for aesthetical reasons and for housing stairs, pipelines, and offices. In this latter case, the whole water supplier building is sometimes considered as a modern architectural heritage piece as a whole [22].

When still in service, water towers represent a critical element in water supply lifelines for both drinking and fire extinguishing. Their collapse in case of extreme events, such as earthquakes, is doubly disastrous because of water distribution interruption and of the consequent risk to cause damage to adjacent buildings. Some of them have instead fallen into disuse as water storage facility and are undergoing restoration for cultural preservation or functional reconversion as touristic attractions [23]. In earthquake prone areas, this includes the challenging task of enhancing the seismic capacity of pre-normative RC structures, subject to a remarkable seismic demand due to the slender configuration and the sloshing water mass on top, while complying with the preservation criteria required when retrofitting heritage buildings.

2.2 Seismic behaviour

Under earthquake base motion, the frame structure supporting the tank is the weakest portion of slender RC elevated water tanks, which, despite their axisymmetric geometry and mass distribution, have proved prone to undesired torsional response [24]. The sloshing water in the tanks, small non-uniformities introduced during construction or developed in time, unsymmetrical position of pipelines, ladders and non-structural elements, and lack of verticality, may cause eccentricities, which, in their turn, and even when small, may activate torsional vibrations [25]. This latter amplifies during seismic base accelerations, increasing localized inelastic displacement demands under hysteretic cycles, possibly leading to the shear failure of RC beams or of beam-to-column joints [26]. Failure of beams in bending and of columns under axial compression have been reported as well [27]. Torsional response is undesired and usually unexpected, making the seismic behaviour of water towers counterintuitively complex. Apart from the limited seismic response requirements foreseen by design codes at the time of construction, many RC elevated water tanks were designed

as perfectly symmetric systems and, based on this assumption, provided with insufficient strength and ductility capacities [28].

Inelastic response amplification may be further increased by lateral-torsional coupling, and the critical range of the torsional-to-lateral vibration period ratio (referred to as τ in the literature) has been estimated between 0.7 and 1.25 [29]. Therefore, with the aim of estimating the seismic vulnerability associated with torsional response of existing tanks, of upgrading the weakest ones, and of designing new ones, appropriate stage configurations have been identified, that include more columns, possibly arranged in a two-concentric layout, radial beams, and diagonal braces to keep τ out of the critical range. Base isolation [26, 30, 31] and damping braces [26, 32, 33] have also been proposed for the seismic protection of existing elevated tanks.

2.3 Structural health monitoring

There is an increasing need of periodically assessing the structural condition of elevated water tanks, due to the strategic role of in-service ones in water supply lifelines, to the architectural value of the dismissed ones, and to the potential threat caused by their collapse. The strength deterioration caused by aging, such as concrete cracking and steel corrosion, contributes to the progressive decrease of their safety level over time. The difficulty of reaching the highest portion of the tower, the presence of adjacent structures, and the limitations to inspection activities on heritage assets, increases the potential for advanced non-invasive technologies.

At the present stage, inspection and control of water towers make use of routine tools. Cover depth measurement and crack pattern survey are carried out to detect concrete deterioration. Half-cell potential, resistivity and chloride content measurements are performed to investigate steel corrosion [34]. These methods provide local information, whilst a global assessment is performed via dynamic monitoring with accelerometers. The installation of these instruments requires costs for their purchase and for the difficulty of reaching the elevated portion of the structure, where they can also hardly be maintained in operational efficiency. Despite the major significance of developing reliable and cost convenient SHM strategies for elevated water tanks, the application of novel contactless techniques [6], recently been made available for the structural dynamic monitoring and condition assessment, has never been investigated to date.

3 Structure under study

3.1 Description of the elevated water tank

The water tank considered in this work is in Rome, Italy, near Tiburtina Railway Station. It was built in the 1960s as part of the water supply network of the East quadrant of the city. Despite it has now fallen into disuse, it still represents a well recognizable element of the skyline of the area, which has recently undergone deep urban renewal. The structure (shown in Figs. 1 and 2) comprises four reinforced concrete columns, having a concrete cross-section of 2.20 m × 0.65 m and, as revealed by non-destructive tests (§3.3), an external brickwork layer of 5 cm, resulting in a total cross-section of 2.30 m × 0.75 m (Fig. 1a). The section of the columns reduces to 1.30 m × 0.65 m at 15.30 m height, where they support a 1.00 m × 2.00 m ring beam and a cylindrical tank with 8.30 m outer diameter and 9.60 m total height, as thoroughly surveyed via aero-photogrammetry (§3.2). The thickness of the side wall and of the base slab was estimated as 0.30 m and 0.45 m, respectively, based on those of similar structures, as original design documents were unavailable and direct inspection was unfeasible. The inner diameter and depth of the tank result in 7.60 m and 7.20 m, respectively. On top, the columns support a RC ring beam with 1.32m × 0.60 m cross-section and a circular roof with cross braces (Fig. 1b). Overall, the structure is 27.95 m high (Fig. 2). A central circular column, having 2.50 m external diameter and 0.25 m estimated thickness, covered with a 5 cm thick brickwork layer, hosts the piping system (Fig. 1c). The structure is founded on a RC slab, partially emerging from the ground (the depth of the footing could not be precisely determined).

3.2 Digital survey

A digital survey was carried out to develop a 3D geometric model, integrating aerial and terrestrial photogrammetry [35–37]. A DJI Mavic Mini drone was used for the aerial survey. The drone has a 12MPx camera, featuring a 6.2 mm × 4.5 mm CMOS sensor, a 4.5 mm focal length lens (24 mm in the full-frame format), and an f/2.8 diaphragm aperture. Approximately 250 4000px × 2250px high resolution photos were taken with the exposure set to Auto ISO mode, in about 40 min.

As the drone camera was unable to tilt upwards by more than 20 degrees and due to the narrow space between the columns supporting the tank, the aerial survey was accompanied by a terrestrial survey, focussing on the bottom part of the tank. The terrestrial survey was carried

Fig. 1 Lateral (**a**), top (**b**) and bottom (**c**) view pictures of Tiburtina elevated water tank

out with a Nikon D610 digital camera, having 24.3MP, a 36 mm × 24 mm CMOS sensor and a 50 mm equivalent focal length. The survey lasted about 20 min, for a total of 100 4512px × 3800px pictures, taken with the ISO sensitivity set at 5000, to reduce digital noise, and an f/14-to-20 aperture of the diaphragm.

Frames were processed in Agisoft Metashape Professional® [38]. A sparse point-cloud of approximately 217.000 points (Fig. 3a) was obtained first, and then a dense cloud of about 14 million points (Fig. 3b) and a 3D textured model (Fig. 3d) were derived. Twelve markers were placed on the columns and on the ground before surveying, which served as scale bars (known distances between predefined pairs of markers) allowing model scaling (conversion from pixel to millimetres).

Both the dense cloud and the textured model were used in the post-processing phase to build up the structural model for numerical simulations (§4.2). The dense cloud was used to derive accurate geometric details, such as total height, size of the two ring beams, shape and dimensions of the circular roof, and reduced sections of the columns at the base of the tank, which would have been undetectable otherwise, due to the height of the construction. The textured model (Fig. 4b), being a faithful digital representation of the construction, provided information on construction details, including the detachment of the tank from the columns along its entire height, implemented in structural modelling (Fig. 4c). Environmental deterioration phenomena were also detected, such as water draining marks (Fig. 4a).

3.3 Non-destructive tests performed in the field

As mentioned above, original design documents were unavailable, so the only information was detected by survey. Moreover, the structure is classified as historic architectural heritage, so destructive or even minimally invasive testing was not allowed. Due to such restrictions, only non-destructive tests were authorized, which were carried out to inspect the inner cross-section of the columns. Georadar and pulse-induction test detected a brickwork

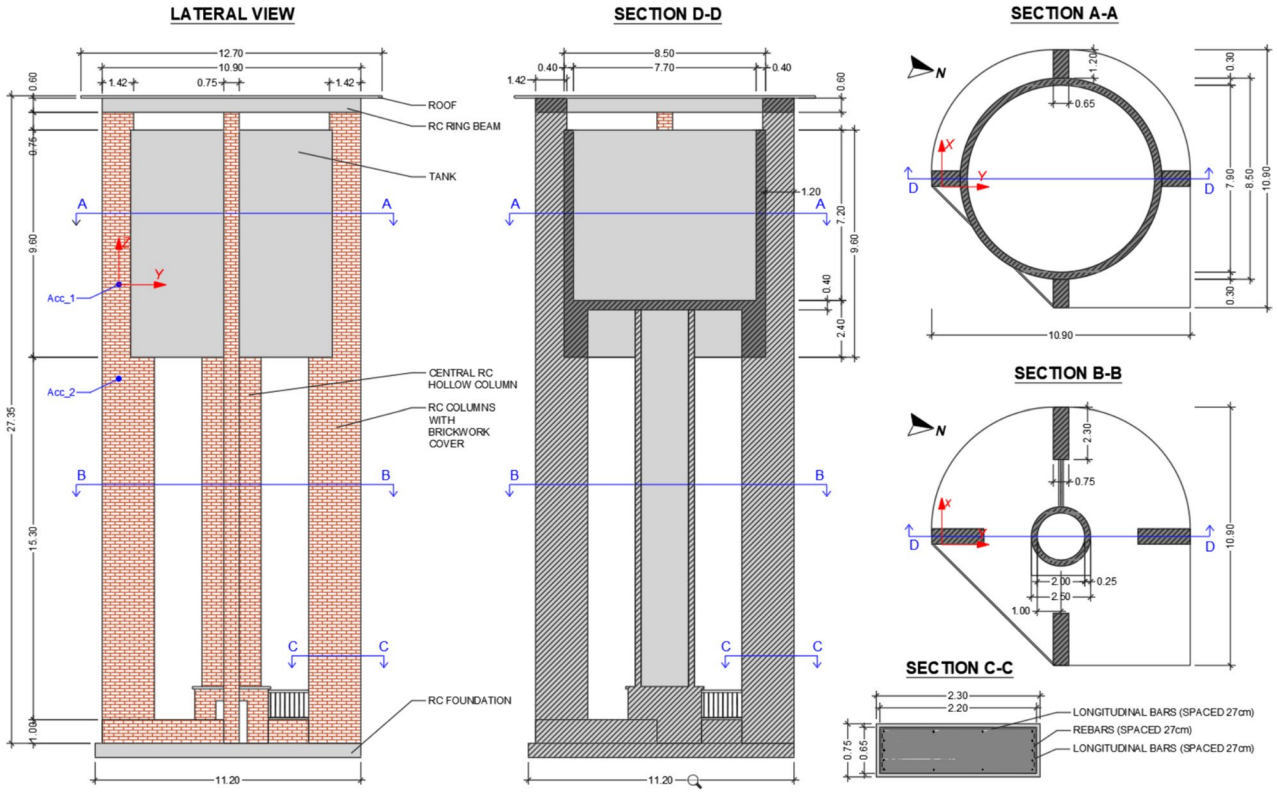

Fig. 2 Lateral view, and vertical and horizontal cross sections of Tiburtina elevated water tank

Fig. 3 Photogrammetric model of Tiburtina elevated water tank: sparse (**a**) and dense (**b**) point clouds, and 3D textured model (**c**)

outer layer of 5 cm thickness and a concrete cover of 3 cm thickness, and, at 8 cm depth, the presence of metal bars (Fig. 5). Two 70 cm spaced longitudinal bars were detected along each long side of the column (Fig. 5a, b) and five 13 ÷ 14 cm spaced longitudinal ones on the short side (Fig. 5c). Shear rebars were 23 ÷ 27 cm spaced (Fig. 5d, e). No reliable measures on bar diameter were obtained. On the other hand, since removal the brickwork layer was not allowed, no tests on concrete could be carried out (not even non-destructive ones). Therefore, no test data were obtained on concrete mechanical properties.

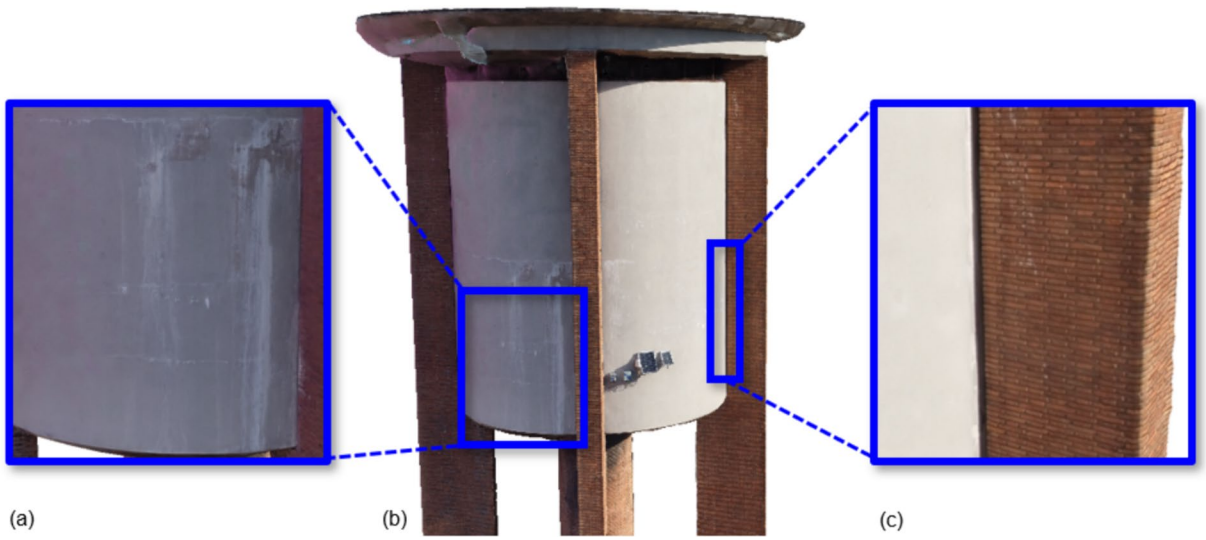

Fig. 4 3D textured model of Tiburtina elevated water tank (**b**) with focus on specific details of water draining (**a**) and tank-to-column discontinuity (**c**)

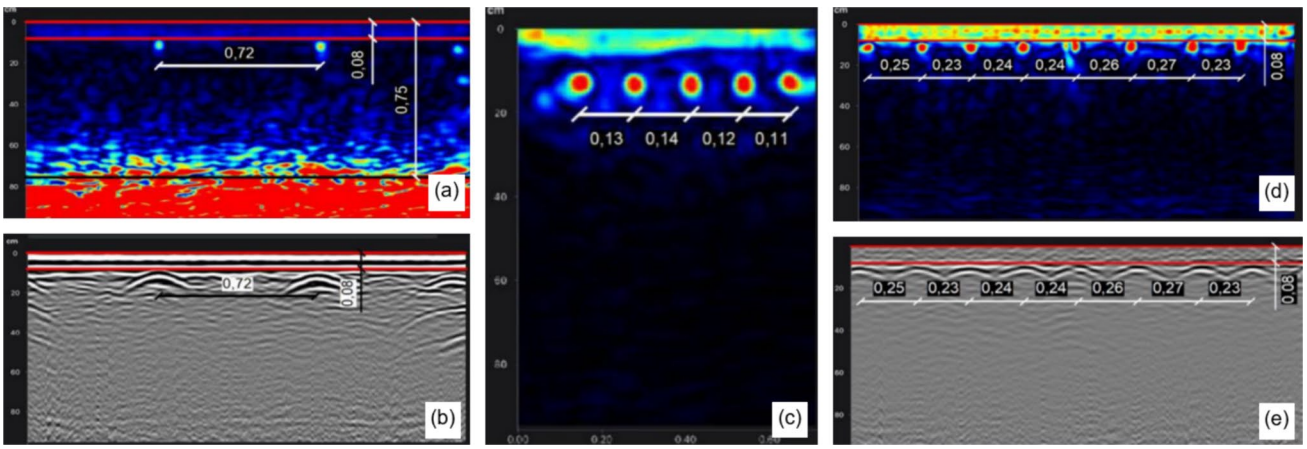

Fig. 5 Georadar detection of longitudinal bars on the long side (**a**, **b**) and on the short side (**c**) and of transversal rebars (**d**, **e**) in the cross-section of the columns

4 Preliminary structural analyses

4.1 Analytical estimate of the fundamental frequency

As a first step, the fundamental frequency of the water tower was estimated analytically through a single-degree-of-freedom (SDOF) system. Since the structure is not in service anymore, it was assumed that the tank was empty. The main geometric information was closely detected, whereas the thickness of the tank side walls and base slab and of the central column was estimated (§3). No field tests were feasible on concrete, so its specific weight and stiffness were not detected, but reasonable values were assigned throughout this study based on construction practice in 1960s.

To calculate the properties of the SDOF system, multiple values were taken for uncertain parameters in the following ranges: the thickness of the tank side wall was varied between 0.20 and 0.40 m, that of the tank base slab between 0.30 and 0.50 m and that of the central column between 0.20 and 0.40 m. As for concrete, the Young's modulus was varied between 20 kN/mm^2 and 25 kN/mm^2, and the unit weight between 23 kN/m^3 and 25 kN/m^3. Either a flexural response or a torsional response was considered for calculating mass and stiffness of the SDOF. As for the former, the four columns were assumed to behave as cantilever beams, all

bending around one of the main axes of the structure, with the tank translating horizontally. The mass (m) of the SDOF system ranged between 570 and 679 ton and its stiffness (k) varied between $928.2 \cdot 10^3$ kN/m and $1090.1 \cdot 10^3$ kN/m, leading to an estimated fundamental frequency (f) comprised between 5.8 and 7.0 Hz. As for the torsional mode, it was considered that each column bend around its weakest axis, with the tank rotating around the vertical axis. The SDOF system had $m = 9.59 \cdot 10^3 \div 11.73 \cdot 10^3$ ton·m^2, $k = 10.1 \cdot 10^3 \div 11.9 \cdot 10^3$ kNm, leading to $f = 4.6 \div 5.6$ Hz. Given the simplifications associated with the representation of the tower as a SDOF system and the uncertainties on some key parameters, the obtained frequencies were taken as preliminary indications and used to orient the following phases of the investigation.

4.2 Numerical simulation

As part of the preliminary study, the natural frequencies of the structure were estimated with a finite element model (Fig. 6a–c). Beam elements were used for the four RC perimeter columns and for the central hollow one. The bottom slab and the side walls of the tank were modelled with shell elements. Finally, the ring beams were modelled as beams. Uncertain geometric and mechanical parameters were varied in the same ranges selected for the abovementioned analytical calculations. The numerical model provided a first fundamental frequency between 4.2 and 5.2 Hz, associated with a torsional mode (Fig. 6d), and a second frequency between 5.0 and 6.2 Hz, associated with two flexural modes, one for each of the two principal directions in the horizontal plane, parallel to the sides of the cross-sections of the columns (Fig. 6e). The significance of the torsional response is consistent with the literature [25–29, 39], because of the arrangement of the four RC columns, which are fixed into the foundation and connected through the ring beam on top. On closer view, in the flexural response of the tower, two columns are engaged around the strong stiffness axis and the other two ones around the weak one. On the contrary, the torsional response involves the engagement of all the columns around the weak axis of their cross-section, making this response the one associated with the smaller frequency.

Despite their approximations, the two simplified approaches followed for analytical calculations and numerical simulations indicated that both the torsional and the flexural responses play a remarkable role in the dynamic behaviour of the tank and provided some ranges for the associated frequencies, which were estimated close to each other, suggesting that the two modal shapes are likely to be coupled.

5 Dynamic monitoring with accelerometers

5.1 Velocity measurements

The railway line and some structures of the area around Tiburtina Rail Station recently underwent renovation works near the elevated water tank. Due to the architectural importance of this structure, local authorities required that the possible effects of the activities carried out in the construction

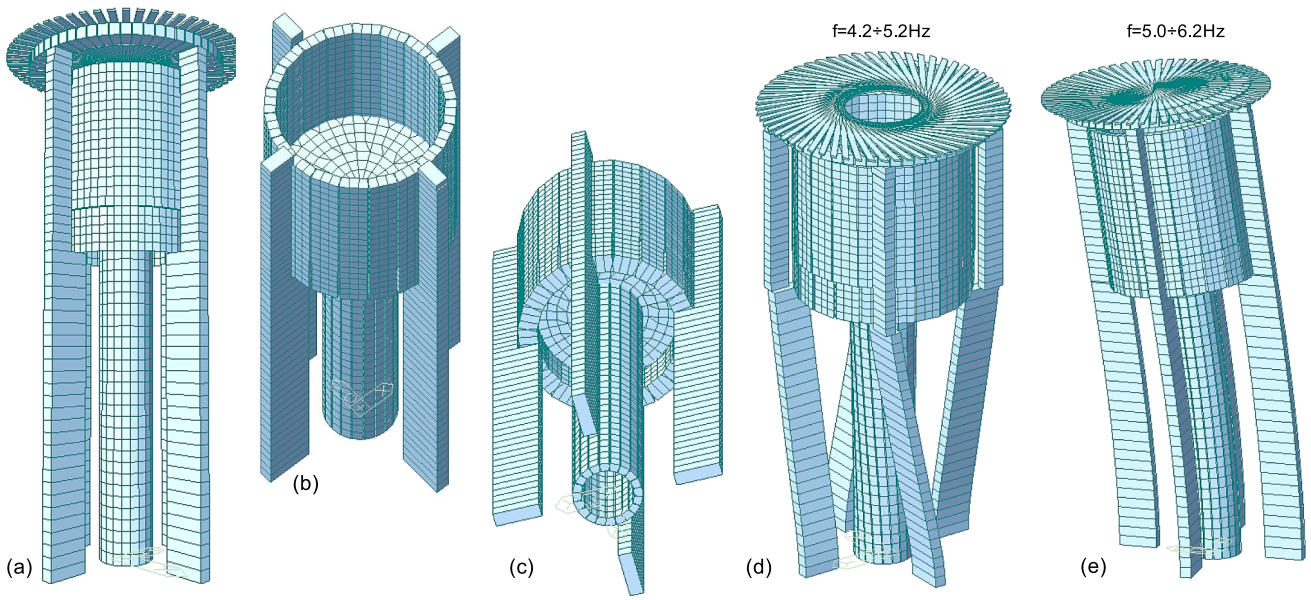

Fig. 6 Overview of the numerical model (**a**), detail of the elevated tank (**b**) and of the cylindrical central columns (**c**), and modal shapes for the torsional (**d**) and flexural (**e**) vibration modes

site were to be kept under control. To this purpose, according to Italian UNI 9916 standard [40], the vibrations were monitored, and velocity peak values were compared to the thresholds associated with the formation or development of damage, mainly cracking of concrete cover or of mortar joints. To this aim, UNI 9916 refers to German DIN 4150–3 code [41], which defines three structural classes, such as industrial, residential, and monumental buildings. In the absence of specific indications for water towers, the structure under investigation was considered as a monumental building, which led to the application of the lowest threshold, equal to 8 mm/s.

Two Ultra-Low-Power (ULP) wireless Micro Electro-Mechanical System (MEMS) triaxial accelerometers were used, having ±2 g range, 660 mV/g sensitivity, and 45 μγ/Hz$^{1/2}$ noise spectral density. Sensors were installed through metals plates and steel screws to one of the columns at 20.0 m (Acc_1) and at 15.5 m (Acc_2) height from the ground level (Fig. 2). The accelerometers were powered by a photovoltaic panel installed on the side wall of the tank and were connected to a router, which transferred data to a server. The accelerometers recorded data at 320 Hz sampling frequency. The one at 20.0 m height was continuously operating, whereas that at 15.50 m started registering when triggered over a pre-determined threshold of 0.05 g. Given the need of providing electric power by a panel, the devices were installed on the South side of the tower. A local reference system was defined, such that the horizontal axes x and y were parallel and orthogonal to the short side of the column, respectively (Fig. 2), whereas the z axis was vertical.

Acceleration time-histories were processed through a second-order baseline correction and a fourth-order Butterworth high-pass filter at 0.1 Hz cut-off frequency, and then integrated to calculate velocities. Velocity analyses (whose details are omitted since they are out of the scope of the paper) revealed peaks of 2 ÷ 3 mm/s in x direction and of 2.5 ÷ 4 mm/s in y direction under environmental noise (associated with traffic and wind). These values were well below the limit recommend by [41]. On the other hand, at the same time of intense working activities in the near construction site, higher values were measured, in few cases up to 12 ÷ 14 mm/s, suggesting that some non-negligible vibrations were caused on the elevated water tank.

5.2 Acceleration measurements

Acceleration time histories were 30 min long (which is the recommended duration in Operational Modal Analyses standard practice) and were processed to calculate the Normalized Power Spectral Density (NPSD). The absence of a recording station at the base of the towers made it impossible to perform an Input/Output dynamic identification. Only output data were available, which are, in principle, affected by the frequency content of the input, unknown in this case. It should be noted that output-only measurements provide reliable information on structural dynamic properties only under stationary input signal. In the present study, the simplifying assumption was inevitably made that working activities in the construction site nearby, traffic, wind, and other environmental noise generated stationary dynamic excitation.

Accelerometer Acc_1 resulted more useful than Acc_2 for dynamic identification purposes because it recorded continuously. The NPSD along x direction clearly shows a first frequency peak at 4.8 Hz, followed by one at 5.8 Hz and a third one at 14.8 Hz (Fig. 7a). The first peaks lie in the ranges estimated analytically (§4.1) and numerically (§4.2), but this recording on its own did not indicate whether

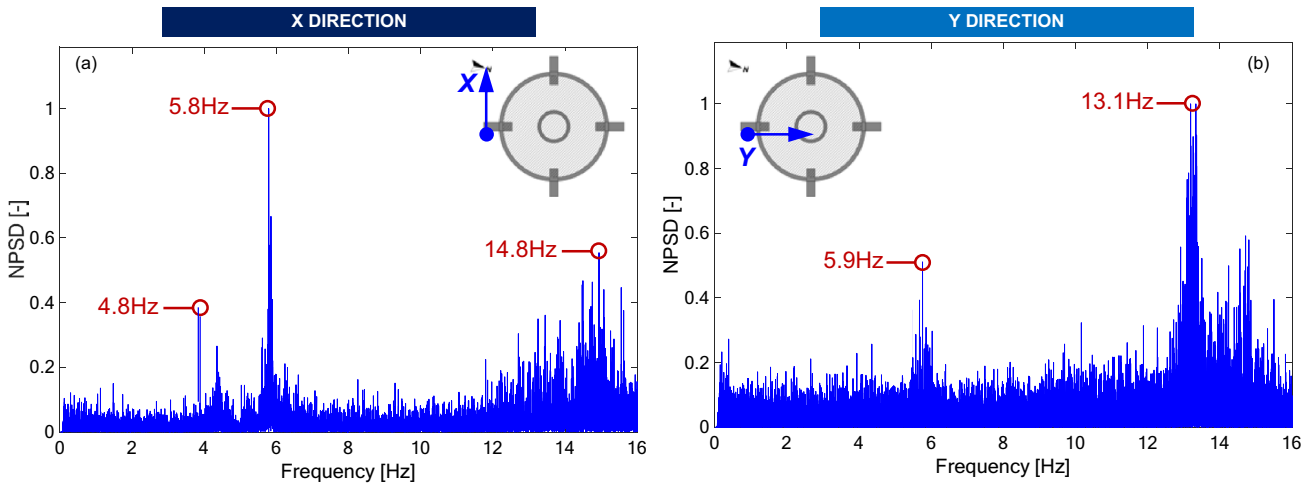

Fig. 7 Normalized Power Spectral Density from accelerations recorded by accelerometer Acc_1 along x (**a**) and y (**b**) directions under environmental noise

such peaks can be associated with a flexural or a torsional response. The processing of the signal in *y* direction showed a frequency peak at 5.9 Hz and one at 13.1 Hz (Fig. 7b), sufficiently close to the frequencies identified in *x* to suggest a correlation, whereas the frequency at approximately 4.8 Hz was not detected. These results alone were considered insufficient, by themselves, to fully characterize the dynamic behaviour of the elevated water tank. The application of the computer-vision-based methodology, described in the following, was then performed to complement these outcomes.

6 Dynamic identification via digital video processing

6.1 Methodology

A strategy to determine the natural frequencies of the structure is proposed, which is based on the post-processing of digital videos recorded with a commercial camera. The method can be either alternative to or combined with traditional measurements for an easier, cheaper and/or improved detection of structural dynamic properties. The methodology consists of the following steps, which make use of authomatized tools and, at the same time, require some engineering judgment and a preliminary qualitative structural analysis for deriving reliable results.

6.1.1 Video recording

First, digital videos of the structure were recorded at a nominal frequency of 60 frames per second (fps), with 1920px × 1080px resolution. A commercial Nikon D610 reflex digital camera was used, but promising results for analogous applications were obtained also with smartphones [42].

As opposed to global shutter cameras, which provide high reliability in computer-vision-based applications, the camera adopted in this study operated in progressive scanning mode, which may cause distortion, skewing of images, blur of motion and temporal aliasing. Among them, given that the analyses were mainly focused on natural frequencies rather than mode shapes, temporal aliasing was considered the most significant one. Aliasing may occur when the structural movement approaches or exceeds the Nyquist limit of the frame rate. For the analysed case, since the main frequencies of the structural response (between 4 and 15 Hz according to accelerometric measurements) were much lower than the Nyquist frequency (30 Hz), temporal aliasing was not expected to occur. It is worth mentioning that the upper-bound limit of 30 Hz associated with the recording frequency of commercial cameras (60fps) is acceptable for civil engineering applications, since structures usually vibrate at lower frequencies, but it may restrict the use of computer vision-based methods in other fields, such as aerospace or mechanical engineering.

Since video acquisition highly affects the overall quality of the dynamic identification analysis, the position of the camera with respect to the target structure needs to be carefully determined having in mind expected mode shapes and associated directions. In the present case, the symmetry of the structure suggested to align the sensor plane either to the *xz* plane or to the *yz* plane (see Fig. 2 for axes orientation). Moreover, it was expected that this would provide results comparable with the ones obtained with the accelerometers, so their direction was also taken into account. Attention was paid to minimize camera vibrations, which would bias the vibrations recorded on the structure. A professional tripod was placed on flat solid ground, far from vegetation, and its legs were firmly grounded on a concrete pavement, cleared from debris. No sensors were attached to the camera to record the amplitude and frequency content of its vibrations, but this was identified as a development step of the methodology. Most of the structure should be included in the frame space to allow a detailed selection of the features to monitor during time, and this required the camera to be at about 20 m from the water tower, also considering the presence of other small buildings, the railway and a construction site, which posed some constraints on camera position. Future investigations will explore the use of telephoto lens to improve the resolution of video frames recorded at large distance from the structure. Finally, lighting conditions should be as constant as possible to minimize noise and, to this aim, videos were recorded in the central hours of a sunny day. More in general, weather conditions may influence the quality of results and they should always be reported to contextualize video recordings. According to local weather reports for the construction site, on the day of video acquisition (25/03/2022), the average wind speed was 5 km/h and its maximum value was 15 km/h, and the average relative humidity of 54% ensured a visibility of 21 km.

Several videos were recorded. The results of two of them are reported and discussed herein, one with the sensor aligned to the *xz* plane (Video-XZ, Fig. 8, recorded at 17 m distance) and one with the sensor aligned to the *yz* plane (Video-YZ, Fig. 9, recorded at 22 m distance). The other videos provided redundant results, or, in few cases, no evident frequency could be derived from them. Videos were cut to a duration of 30 s, by removing the initial and the final parts in which the camera was turned on and off and, therefore, possibly moved. Each video had $n = 1800$ frames, corresponding to its duration in seconds times the acquisition frequency in frames per second (fps). Video duration of 30 s translated in a frequency resolution of 0.034 Hz, which was considered acceptable for the purpose of this study. Longer videos should have been recorded to improve resolution, at

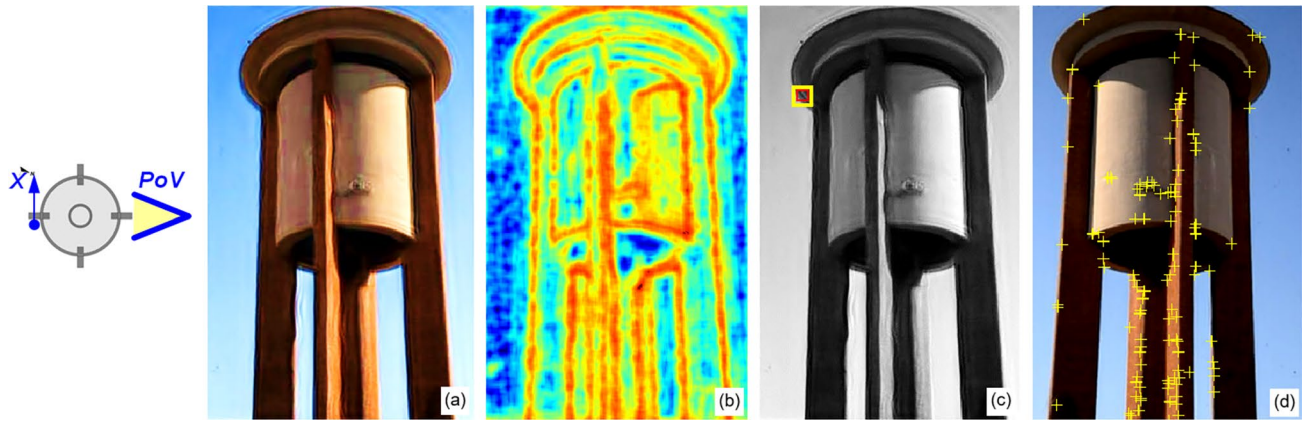

Fig. 8 Frame of magnified video (**a**), entropy map (**b**), selected region of interest (ROI) for grey-intensity variation analysis (**c**) and selected pixels for position tracking analysis (**d**) of Video-XZ

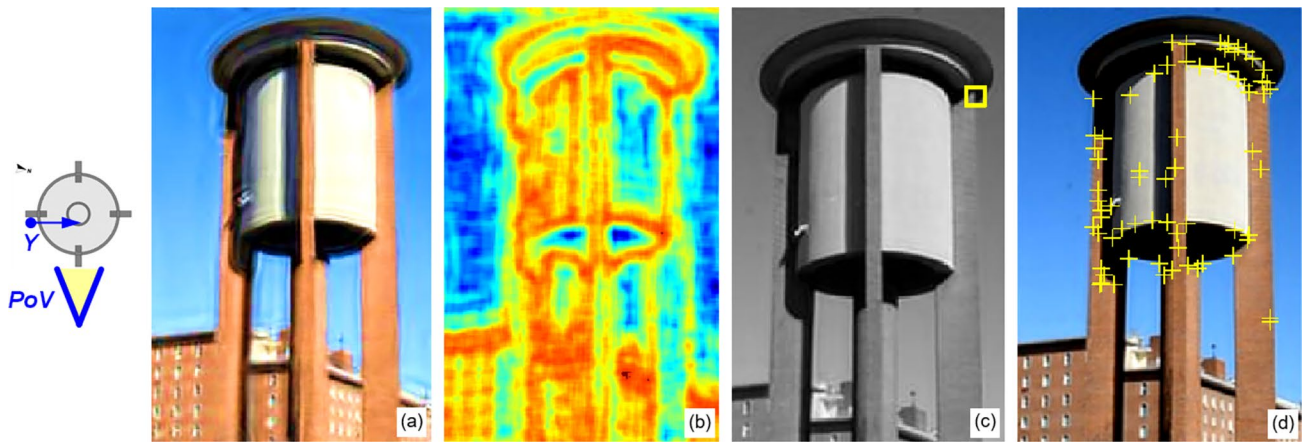

Fig. 9 Frame of magnified video (**a**), entropy map (**b**), selected region of interest (ROI) for grey-intensity variation analysis (**c**) and selected pixels for position tracking analysis (**d**) of Video-YZ

the cost of longer runtimes for their post-processing. This issue would deserve attention in future studies.

Based on recorded digital videos, displacements were detected in pixel. In raw data, the smallest measurable displacement corresponded to pixel dimension, which depends upon sensor resolution and distance from the structure and were $13 \div 16$ mm in this case. Sub-pixel interpolation algorithms were applied to improve accuracy up to 1/100 of a pixel [43].

6.1.2 Motion magnification

Civil structures generally exhibit small amplitude vibrations under environmental noise, which are invisible to the naked eye, nor can be detected in a recorded video as is. A relatively newly formulated technique called motion magnification [5] has recently become available to open source, which amplifies the motion of an object by a pre-determined factor α. Motion magnification algorithms have been used in several fields of experimental physics and mechanics, and their application has proved advantageous for the dynamic identification of civil structures [15–17, 44–48]. The amplification factor α is set together with a range of frequencies, expected to be relevant for the structure. The mathematical formulation and the details of this algorithm are extensively discussed in the literature [5, 49–52] and are omitted herein for brevity.

Before motion magnification processing, cut videos were cropped to a frame size in which the structure is clearly visible and most of the surrounding objects are excluded from the frame. If included, surrounding objects would entail additional and unnecessary computational cost in the magnification process. Frames shown in Figs. 8, 9 are cropped. Then, videos were magnified with an amplification factor $\alpha = 40$ within the $3 \div 16$ Hz frequency range, which included the most relevant vibration modes according to the analytical

estimates, numerical simulations and acceleration recordings described beforehand.

6.1.3 Grey intensity variation and displacement tracking analyses

Magnified videos were divided into n frames and post-processed with an in-house software in Matlab® language. To derive information on the motion of the elevated water tank, either the grey-intensity variation of the pixels in a selected region of interest (ROI) or the displacement of a set of pixels were monitored.

The former case (when grey-intensity variation is monitored) consists of a Eulerian approach, which does not provide specific correlation between the signal and the direction of motion. The latter case (when pixel displacement is tracked) consists of a Lagrangian approach, which allows the detection of the directional nature of the signal and, in principle, can thus provide information on structural modal shapes. If only the fundamental frequencies are needed, the direction of motion is not considered, and the two approaches are equivalent.

In the pixel grey-intensity variation analysis (Eulerian approach), video frames were first converted into greyscale images, such that a value between 0 (black) and 255 (white) was attributed to each pixel. Then, a ROI was selected based on image entropy, which is sought to be a suitable means for identifying highly detectable pixels of video frames [15]. Entropy is a statistical quantity interpreted as the probability of a pixel to be surrounded, in a 9px × 9px area centred on it, by pixels with different grey intensity. Selecting pixels in an area with high entropy would ensure a high signal-to-noise ratio and, therefore, an efficient identification. The entropy maps of Video-XZ and Video-YZ are shown in colour maps of Figs. 8b and 9b, in which orange–red identifies high entropy areas, whilst blue identifies low entropy areas. Selected ROIs are shown in Figs. 8c and 9c. The number of tracked points ($m = 100$ for both Video-XZ and Video-YZ) corresponds to the number of pixels in the ROI, such that m time histories of n values each were obtained, describing the variation of grey intensity of each pixel with respect to its initial value (Figs. 10a and c). Data were conveniently organized in a matrix containing m columns and n rows.

In the pixel position tracking analysis (Lagrangian approach), the pixels to track are usually selected at the edges of the structure, where high contrast is expected. A preliminary identification of pixels to monitor was automatically made using the point tracker object available in Matlab®, based on the Kanade-Lucas-Tomasi feature-tracking algorithm [53]. Then, only the points belonging to the structure and considered meaningful for the investigation of its vibrations were manually selected (Figs. 8d and 9d), whilst the others were discarded. The total number of tracked points was named as m, such that the analysis provided m displacement time histories ($m = 118$ for Video-XZ and $m = 98$ for Video-YZ) of n values each (Fig. 10b and d), organized, as above, in an $n \times m$ matrix. Displacements were detected in pixels; they could be converted into millimetres through a pixel-to-millimetre conversion factor, but it was unnecessary in the present case, since the extent of vibrations was not under investigation.

Time histories were filtered using a symmetric Hamming window function, which attenuates the signal at its edges (initial and final portions) and makes the start and end of the sample match. This expedient is particularly useful to improve accuracy of frequency detection when the original signal is cut to a shorter portion (window) [54, 55]. Hamming window is applied in signal processing to reduce the spectral leakage that may occur when analysing a finite segment of a signal in the frequency domain using the Fourier Transform. Spectral leakage refers to the spreading of signal energy across multiple frequency bins, making it difficult to identify the true spectral components. Hamming windowing is clearly seen in the time histories in Fig. 10, in which the lateral portions are smoothed to zero and the peak values are in the central part.

As it is seen in Fig. 10b, d, the magnitude of detected displacements differed in the two videos, due to the different selection of pixels to track. Nonetheless, as said before, the frequency content of recorded signals rather than their peak values was important in this case.

6.1.4 Dimensionality reduction through correlation analysis and principal component analysis

The time histories resulting from grey intensity variation and displacement tracking analyses were unavoidably affected by noise and not all of them were fully representative of the motion of the water tower. To select only the time histories that are sought to carry meaningful information on the dynamic properties of the structure, a further post-processing step was introduced. The procedure assumed that the most significant components are the most correlated ones, whereas those associated to noise are the most randomly varying.

Correlation analysis is a powerful technique to filter out noise and isolate the most significant signals in a dataset. It relies on correlation, which measures the degree of similarity or linear relationship between two signals. By comparing the signal of interest to a reference signal (usually referred to as a template or a filter), correlation analysis enhances the signal-to-noise ratio and extract the desired information while suppressing noise. This technique leverages the statistical properties of noise (uncorrelated or weakly correlated) and the desired signals (strongly

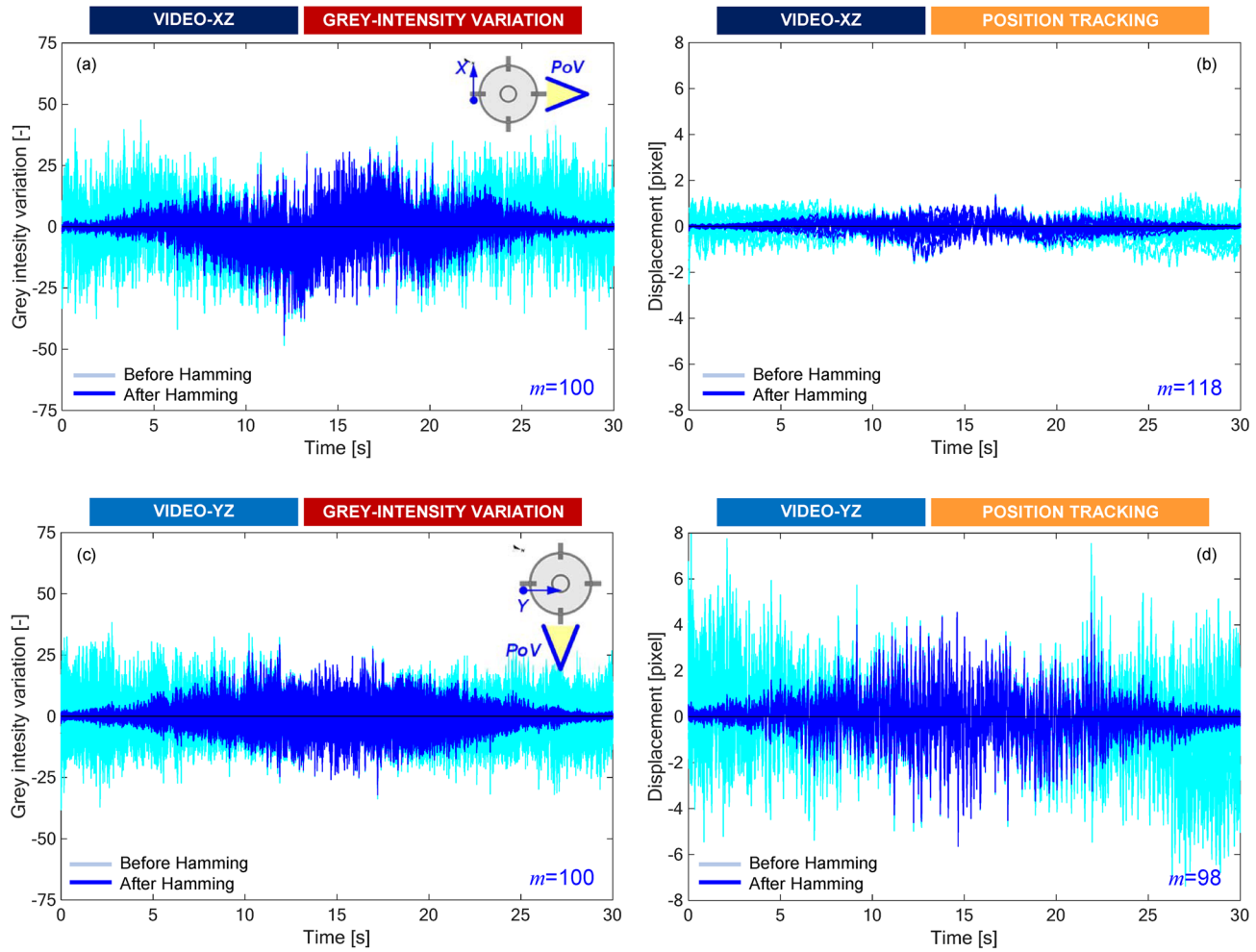

Fig. 10 Time histories of pixel grey-intensity variation (**a**, **c**) and of pixel position tracking (**b**, **d**) analyses for Video-XZ (**a**, **b**) and for Video-YZ (**c**, **d**)

correlated) to enhance the meaningful information while attenuating noise components [56, 57].

First, an $m \times m$ correlation matrix was built, in which each (i,j) entry was the correlation coefficient between the i-th and the j-th time histories and ranged from 0 (uncorrelated signals) to 1 (fully correlated signals). Clearly, the correlation coefficient was equal to 1 on the main diagonal, reporting the correlation of a signal with itself. Then, a threshold was set equal to 0.8, such that only signals with a correlation coefficient above 0.8 were selected, whilst the others were disregarded. Previous sensitivity studies [58] showed that 0.8 is a convenient value for these applications. Lower threshold values would leave insignificant signals (mainly noise) in the post-processing flow, whereas higher threshold values would delete meaningful signals, leading to an uncomplete description of the structural response. After this step, the initial set of m time histories was reduced, for Video-XZ, to $p = 86$ (grey-intensity variation) and $p = 97$ (position tracking) and, for Video-YZ, to $p = 78$ (grey-intensity variation) and $p = 69$ (position tracking).

To further reduce the computational demand, a principal component analysis (PCA) was performed, which is an efficient tool to orient large sets of data to obtain the most relevant information they carry [59, 60]. To apply PCA, time histories were first normalized to 1 and then projected on the principal axes of the $p \times p$ covariance matrix, which represented the covariance of original time histories with respect to each other.

Since variables with larger scales than others may dominate PCA results, they are normalized to a common scale, ensuring that each variable contributes equally to the analysis. Normalizing signals before PCA is, therefore, essential to ensure that the analysis is not biased by differences in variable scales, to obtain interpretable results, and to make the analysis more robust and consistent.

The meaning of the mathematical quantities into play is the following: normalized projected time histories were the

principal components; the eigenvectors of the covariance matrix were its principal axes; and, finally, its eigenvalues represented the amount of information contained in the principal components on the dynamic behaviour of the water tank, that is, the amount and significance of information carried by a signal was associated with its eigenvalue. For an easier representation and comparison, percentage cumulative variance associated with each i-th principal component was calculated as the i-th eigenvalue divided by the sum of all eigenvalues, times 100. Principal components were sorted by percentage information as shown in Fig. 11, and only the first q ones were kept, such that the sum of their percentage cumulative variance was at least 90%, as suggested in the literature [61, 62].

For the dynamic identification of Tiburtina elevated water tank, q resulted equal to 3 for the grey-intensity and displacement variation analyses on Video-XZ and for the displacement variation analyses on Video-YZ, whilst $q=5$ for the grey-intensity variation analysis on Video-YZ. PCA analyses, therefore, led to a significant reduction of the number of signals to post-process in the frequency domain. Each principal component was a signal including n data (it had the same length of original time histories) but different physical dimensions. For instance, the principal component derived from displacement tracking time histories had the dimensions of a squared length.

6.1.5 Inverse transformations and final set of time histories

Finally, the q principal components underwent the inverse transformations to derive as many time histories (Fig. 12), having the same physical meaning (and the same physical dimensions) of original (recorded) ones but being different from the original signals. Hamming windowing was unnecessary for this set of new time histories, which were collected in $n\times q$ matrices. NPSD was calculated on these time histories to identify the dominant frequencies of motion.

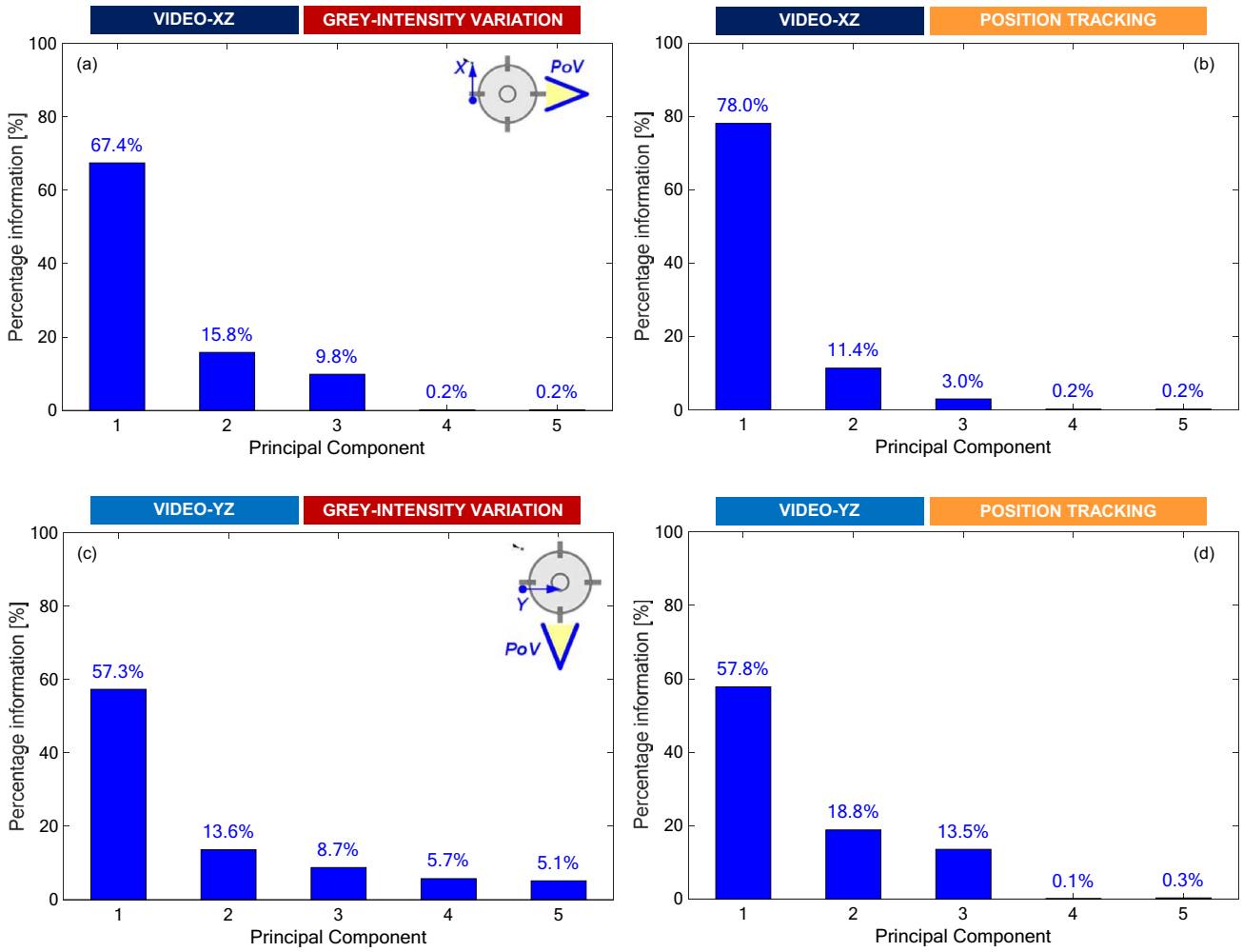

Fig. 11 Content of the first five principal components form pixel grey-intensity variation (**a**, **c**) and from pixel position tracking (**b**, **d**) analyses for Video-XZ (**a**, **b**) and for Video-YZ (**c**, **d**)

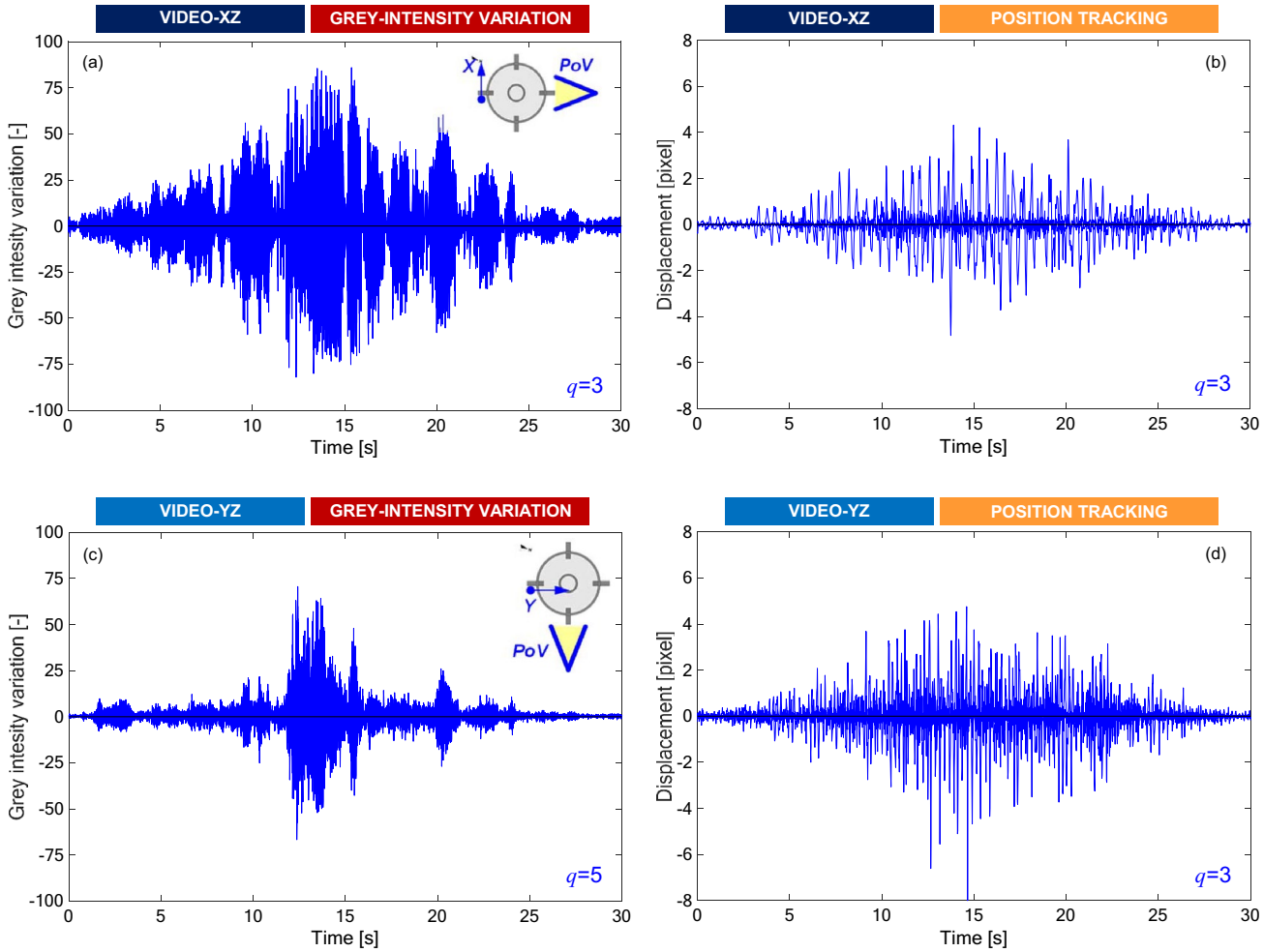

Fig. 12 Final sets of time histories for pixel grey-intensity variation (**a**, **c**) and for pixel position tracking (**b**, **d**) analyses for Video-XZ (**a**, **b**) and for Video-YZ (**c**, **d**)

6.2 Results

6.2.1 Fundamental frequencies

The frequencies extracted from digital video processing were compared to those detected from accelerometric signals and to those estimated by analytical and numerical predictions, aiming at validating the proposed computer vision-based SHM methodology and at improving the insightful interpretation of the dynamic behaviour of the elevated water tank.

Both Video-XZ (Fig. 13a, b) and Video-YZ (Fig. 13c, d) showed the presence of two dominant frequencies, at about 4 Hz (visible only through grey intensity variation analyses) and at about 6 Hz (clearly detectable also in pixel position tracking analyses).

The first peak (at about 4 Hz) was representative of the same first torsional mode of vibration, detected from the two different perspectives. First, this was deduced from numerical simulations. Second, it was inferred observing that the accelerometer in the y direction installed on the structure did not provide any results related to this mode, whose motion components are paralleled to the short side of the cross-section of each column.

The second peak detected at about 6 Hz in both videos and through both analysis approaches was associated to flexural modes of vibration. Both videos were likely to show the two flexural modes, along x and y directions, whose vibration frequencies are similar (5.9 Hz in x and $6.1 \div 6.2$ Hz in y) due to the symmetry of the structure. Finally, a peak at about 14 Hz was detected in Video-XZ (Fig. 13a, b), which was associated with the same higher mode of vibration along x indicated also by accelerometric measurements.

The mismatch between natural frequencies detected from accelerometric measurements and from video processing resulted less than 10% and was likely related to environmental conditions such as light variations and motion of the camera, which, in real field applications, are to some extent

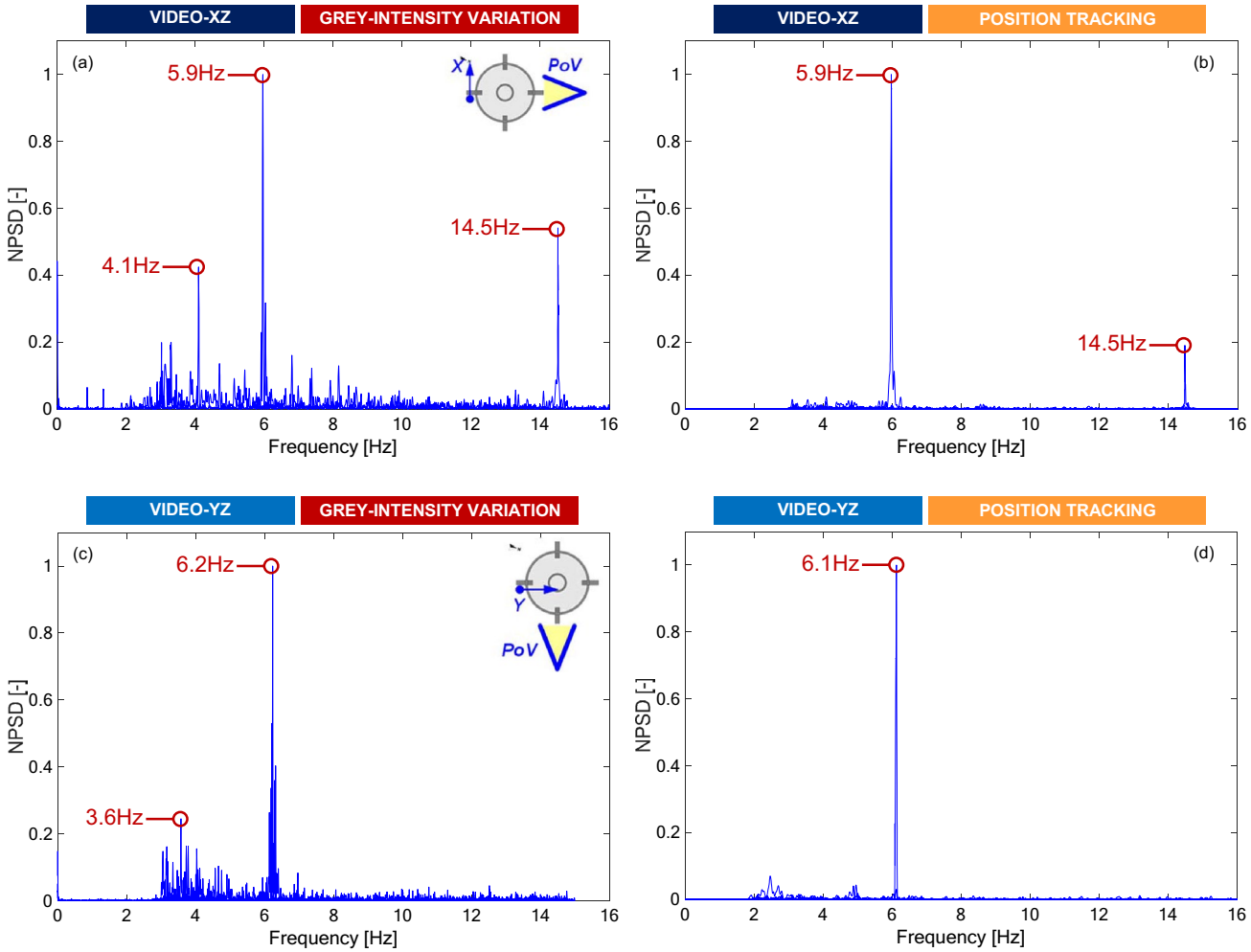

Fig. 13 Normalized Power Spectra Density for pixel grey-intensity variation (**a**, **c**) and for pixel position tracking (**b**, **d**) analyses for Video-XZ (**a**, **b**) and for Video-YZ (**c**, **d**)

unavoidable and are expected to affect the results much more than in laboratory tests.

6.2.2 Vibration modes

To confirm the torsional nature of the first vibration mode emerging from the NPSD plots, accelerometric measurements and numerical simulations, additional analyses were performed, driven by the considerations that, in a torsional vibration mode, the horizontal movements are tangent to the structure, and, when frames are processed, displacement vectors belong to the plane of the analysis in the central portion of the structure whilst being orthogonal to the plane of the analysis in the lateral portions. Therefore, since the projections of displacement vectors on the plane of the video frames are considered, the resulting displacement magnitude in the centre would result larger than those on the sides, which, however, should not be expected to be exactly null due to both possible coupled flexural vibration modes and unavoidable misalignments.

Two advantageous features of the proposed computer vision-based technique were exploited, such as the possibility to perform selective magnification to inspect the structural response within a specific frequency range, and the opportunity to isolate a particular portion of the structure to monitor, through a convenient choice of the pixels to track in the post-processing phase. Furthermore, position tracking analyses were performed to derive information on the direction of motion, which is unavailable if pixel grey-intensity variation is analysed.

First, videos taken from the two abovementioned viewpoints (planes XZ and YZ) were amplified with a magnification factor $\alpha = 40$ in the $3 \div 5$ Hz frequency range, which includes only the first frequency ($3.6 \div 4.1$ Hz), tentatively attributed to the torsional vibration mode, leaving out the second one ($5.9 \div 6.2$ Hz), arguably associated with a flexural mode. Specific markers were selected on different areas

of the water tower, namely on the left, on the centre, and on the right, and both on the columns and on the tank, and video frames were processed following the same procedure described above, to extract the time-histories of horizontal displacements shown in Fig. 14 a,c,e for the XZ plane and in Fig. 15a, c, for the YZ plane. From both viewpoints, the magnitude of displacements exhibited by the central portion of the water tower (Figs. 14c and 15c) resulted one order of magnitude larger than those calculated for its sides (Figs. 14a, e and 15a, e), confirming the torsional nature of the structural vibrations in the isolated and magnified frequency range.

Second, the same two videos were pre-processed again, but this time motion magnification ($\alpha = 40$) was performed in the $5.5 \div 6.5$ Hz frequency range, to include the second peak, tentatively associated with a flexural vibration mode. The resulting time histories of the horizontal displacement of pixels selected on the left, on the central, and on the right portions of the elevated water tank showed a similar amplitude (Figs. 14b, d, f and 15b, d, f). This was considered the conclusive proof of the inferred dynamic identification and, therefore, the first frequency identified in Fig. 13 ($3.6 \div 4.1$ Hz) can be confidently attributed to a torsional vibration mode and the second one to a flexural one, as predicted by numerical simulations.

7 Conclusions

The dynamic behaviour of a reinforced concrete elevated water tank was investigated through a computer vision-based method. Digital videos were recorded by a commercial reflex camera, post-processed and filtered, which also included motion magnification to improve accuracy, given the small vibrations exhibited by the structure under environmental noise. Videos were analyzed both by monitoring pixel grey-intensity variation and by tracking pixel position. When the variation of the grey-intensity was monitored, pixels were selected within a region of interest defined in the area of the frame images with high entropy. In both cases, principal component analysis was applied to reduce computational costs while keeping only the signals carrying the most meaningful information on the dynamic behaviour of the water tower.

Following previous laboratory studies, which provided first validations and suggested useful calibration parameters, in the present research the proposed methodology resulted reliable also in real field applications at the scale of engineering structures, in which stability and light conditions could not be strictly controlled. The two approaches (grey-intensity variation and displacement tracking analyses) provided consistent outcomes, which also agreed with the frequencies detected by two accelerometers placed on the tank and with those estimated by analytical and numerical simulations.

These latter ones were based on information detected by digital survey for geometric detection and by field tests for material characterization but needed some assumptions on the modulus of elasticity of concrete (which could not be determined experimentally), on the actual state of the water tank (it was assumed to be empty), and even on some dimensions which could not be surveyed. Therefore, they could only provide a preliminary estimate of the frequency, but helpfully suggested the parameters for motion magnification (the frequency window in which motion was amplified) and highlighted the possible activation of a torsional mode, which was not recognizable with accelerometers.

In the structure under investigation, two frequency peaks were identified at $3.6 \div 4.1$ Hz and at $5.9 \div 6.2$ Hz that were tentatively attributed to a torsional and to a flexural vibration mode, respectively. To develop a deeper insight on the dynamic behaviour of the water tower, videos were re-processed specifically to confirm the torsional nature of the first vibration mode and the flexural nature of the second one, greatly benefitting from the possibility of the proposed computer vision-based method of recording videos from several positions on the ground, of selecting measurement points in the post-processing phase, of performing selective magnification to inspect the structural response within a specific frequency range, and, finally, of deriving information on the direction of motion through position tracking analyses. The proposed methodology is cheap (relatively inexpensive hardware is needed), totally non-invasive, and versatile. Results were derived from short videos (30 s), allowing for fast field operations and time-saving post-processing, and agreed with the ones obtained from 30 min accelerometric recordings. This indicates that the method is suitable for SHM applications in everyday engineering practice and can be confidently used with accessible equipment and computational tools.

Additionally, computer vision-based analyses provided useful outcomes, unavailable otherwise, which integrated information obtained through routine approaches (namely numerical and analytical previsions, and accelerometric measurements, to date used almost exclusively in engineering practice), and significantly enriched the description of the dynamic properties of the structure under investigation, with a completely marker-free approach.

Computer-vision technologies in real applications require that vibration of the sensor, light and wind conditions in the monitoring area, type of camera and shutter mode, and frequency of acquisition are considered. In this work, drawbacks related to the nature of the shutter were irrelevant, time aliasing was excluded, and results were considered marginally affected by support vibrations, but good practice

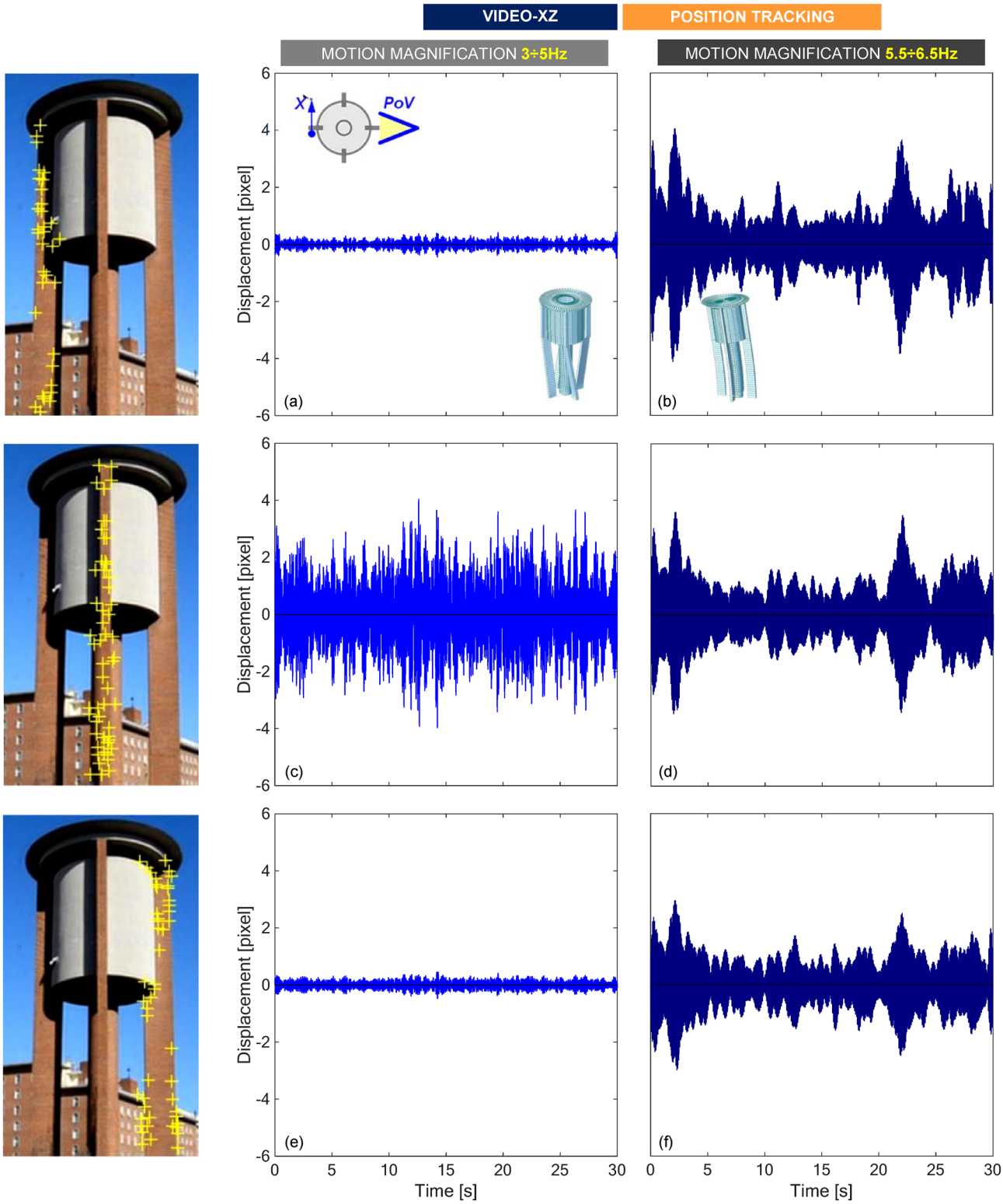

Fig. 14 Time histories of horizontal displacements derived from pixel position tracking analyses on Video-XZ, amplified in the frequency range 3÷5 Hz, for pixels selected in the left (**a**, **b**), central (**c**, **d**) and right (**e**, **f**) portions of the elevated water tank, amplified in the frequency ranges 3÷5 Hz (**a**, **c**, **e**) and 5.5÷6.5 Hz (**b**, **d**, **f**)

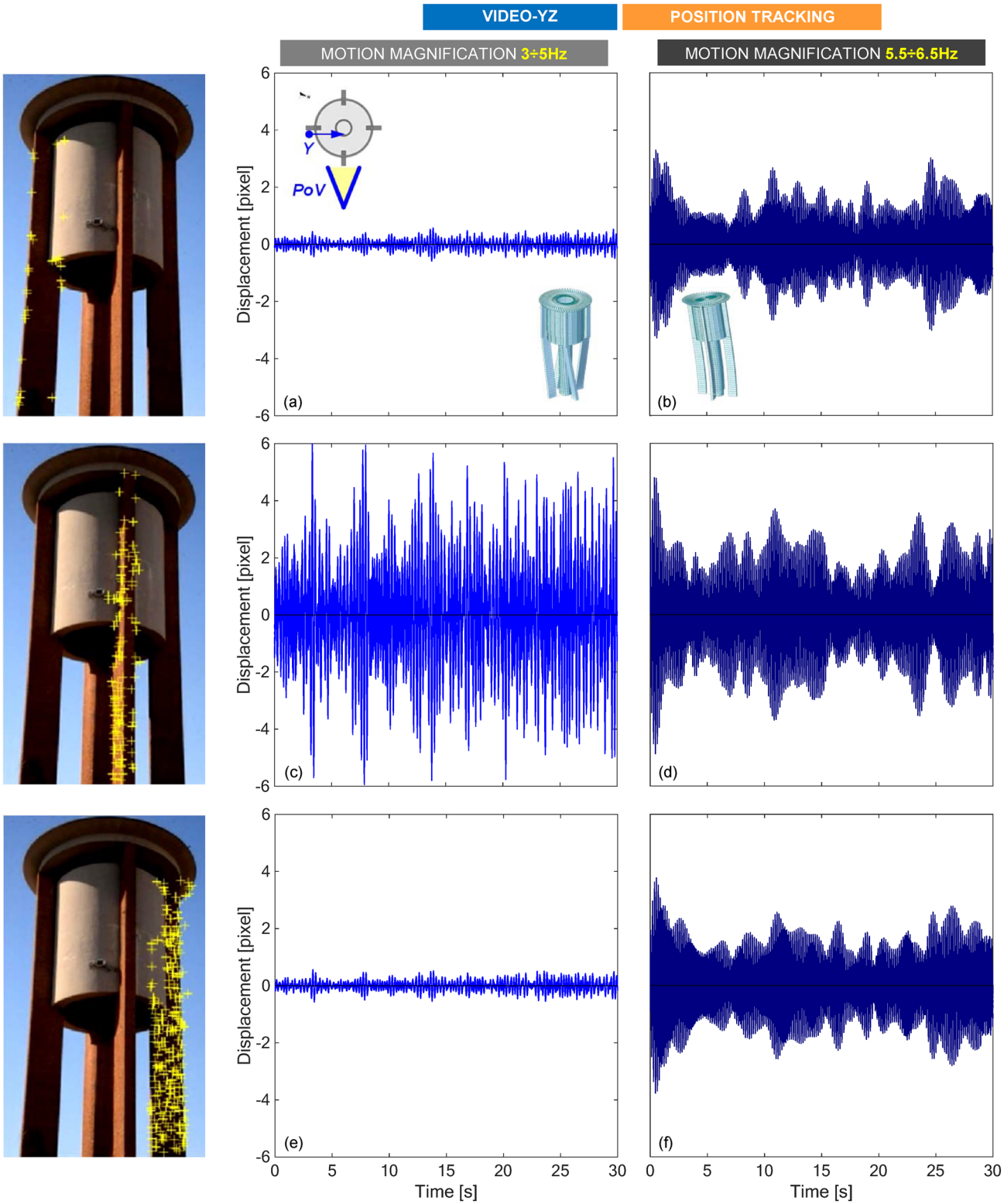

Fig. 15 Time histories of horizontal displacements derived from pixel position tracking analyses on Video-YZ, amplified in the frequency range 3 ÷ 5 Hz, for pixels selected in the left (**a**, **b**), central (**c**, **d**) and right (**e**, **f**) portions of the elevated water tank, amplified in the frequency ranges 3 ÷ 5 Hz (**a**, **c**, **e**) and 5.5 ÷ 6.5 Hz (**b**, **d**, **f**)

would entail the installation of an additional sensor on the camera support to filter undesired vibrations and noise.

Motion magnification still requires some engineering judgment to set the frequency range, but results show that, if appropriately selected, this can effectively serve the investigation of the structural behaviour in a targeted way. Directional features of the motion were not extracted but would, in principle, complement the analyses with information on mode-shapes and amplitude. To do so, however, image blur, skewing and distortion would need to be mitigated resorting to expensive acquisition equipment (global shutter cameras, possibly in stereo mode, with larger sensors and higher resolution).

Although more research is still needed to promote the affordable use of computer-vision-based methodologies in everyday engineering practice, scientific outcomes indicate that they have huge potential for structural health monitoring. At the present state of knowledge, their application is feasible in combination with traditional measurement approaches, whereas complete replacement appears still far-fetched.

Acknowledgements This work was carried out within the Research Projects "STima e ANalisi del Danneggiamento di edifice storici indotto da opere in sotterraneo (STAND)" and "Integrated systems for the seismic retrofitting of architectural heritage (RIPARA)" funded by Regione Lazio, and within the Research Project "Cultural Heritage Active Innovation for next-gen sustainable society (CHANGES)" funded by the National Recovery and Resilience Plan (NRRP), Mission 4, Component 2, Investment 1.3 supported by the "Next Generation EU" Programme of the European Union. The collaborative support of the staff of Indagini Strutturali srl is gratefully acknowledged.

Funding Open access funding provided by Università degli Studi Roma Tre within the CRUI-CARE Agreement. Regione Lazio, A0375-2020-36637, Gianmarco de Felice, 305-2020-35586-25/05/2020, Gianmarco de Felice.

Data availability Data and source code are available upon request to the corresponding author.

Declarations

Conflict of interest The authors declare that there are no known competing financial interests or personal relationships that could have appeared to influence the work reported in this paper.

References

1. Sony S, Laventure S, Sadhu A (2019) A literature review of next-generation smart sensing technology in structural health monitoring. Struct Control Health Monit 26:e2321. https://doi.org/10.1002/stc.2321
2. Lofrano E, Paolone A, Ruta G (2020) Dynamic damage identification using complex mode shapes. Struct Control Health Monit 27:e2632. https://doi.org/10.1002/stc.2632
3. Lofrano E, Pingaro M, Trovalusci P, Paolone A (2020) Optimal sensors placement in dynamic damage detection of beams using a statistical approach. J Optim Theory Appl 187:758–775. https://doi.org/10.1007/s10957-020-01761-3
4. Fukuda Y, Feng MQ, Shinozuka M (2010) Cost-effective vision-based system for monitoring dynamic response of civil engineering structures. Struct Control Health Monit 17:918–936. https://doi.org/10.1002/stc.360
5. Wadhwa N, Rubinstein M, Durand F, Freeman WT (2013) Phase-based video motion processing. ACM Trans Graph 32(1):10. https://doi.org/10.1145/2461912.2461966
6. Feng D (2018) Feng MQ Computer vision for SHM of civil infrastructure: from dynamic response measurement to damage detection – a review. Eng Struct 156:105–117
7. Bhowmick S, Nagarajaiah S, Lai Z (2020) Measurement of full-field displacement time history of a vibrating continuous edge from video. Mech Syst Signal Process 144:106847
8. Ye X-W, Jin T, Ang P-P et al (2021) Computer vision-based monitoring of the 3-D structural deformation of an ancient structure induced by shield tunneling construction. Struct Control Health Monit 28:e2702. https://doi.org/10.1002/stc.2702
9. Silva MF, Green A, Morales J et al (2022) 3D structural vibration identification from dynamic point clouds. Mech Syst Signal Process 166:108352. https://doi.org/10.1016/j.ymssp.2021.108352
10. Jana D, Nagarajaiah S, Yang Y (2022) Computer vision-based real-time cable tension estimation algorithm using complexity pursuit from video and its application in Fred-Hartman cable-stayed bridge. Struct Control Health Monit 29:e2985. https://doi.org/10.1002/stc.2985
11. Xu Y, Brownjohn JMW (2018) Review of machine-vision based methodologies for displacement measurement in civil structures. J Civil Struct Health Monit 8:91–110. https://doi.org/10.1007/s13349-017-0261-4
12. Kumar D, Chiang C-H, Lin Y-C (2022) Experimental vibration analysis of large structures using 3D DIC technique with a novel calibration method. J Civil Struct Health Monit 12:391–409. https://doi.org/10.1007/s13349-022-00549-5
13. Prasad S, Chiang C-H, Kumar D et al (2023) Robust and efficient feature-based method for structural health monitoring of large structures. J Civil Struct Health Monit 13:961–982. https://doi.org/10.1007/s13349-023-00686-5
14. Yang Y, Nagarajaiah S (2014) Blind identification of damage in time-varying systems using independent component analysis with wavelet transform. Mech Syst Signal Process 47:3–20. https://doi.org/10.1016/j.ymssp.2012.08.029
15. Fioriti V, Roselli I, Tatì A et al (2018) Motion magnification analysis for structural monitoring of ancient constructions. Measurement 129:375–380. https://doi.org/10.1016/j.measurement.2018.07.055
16. Civera M, Zanotti Fragonara L, Antonaci P et al (2021) An experimental validation of phase-based motion magnification for structures with developing cracks and time-varying configurations. Shock Vib 2021:1–16. https://doi.org/10.1155/2021/5518163
17. Wangchuk S, Siringoringo DM, Fujino Y (2022) Modal analysis and tension estimation of stay cables using noncontact

vision-based motion magnification method. Struct Control Health Monit 29:e2957. https://doi.org/10.1002/stc.2957
18. Cataldo A, Roselli I, Fioriti V et al (2023) Advanced video-based processing for low-cost damage assessment of buildings under seismic loading in shaking table tests. Sensors 23:5303. https://doi.org/10.3390/s23115303
19. Sangirardi M, Altomare V, de Felice G (2021) Analysis of the dynamic response of a masonry wall through computer vision and image processing techniques. In: Proceedings of the 10th international conference on structural health monitoring of intelligent infrastructure (SHMII-10), Porto, Portugal
20. Sangirardi M, Altomare V, De Santis S, de Felice G (2022) Detecting damage evolution of masonry structures through computer-vision-based monitoring methods. Buildings. https://doi.org/10.3390/buildings12060831
21. Hughes S (2018) TICCIH, ICOMOS & The World Heritage. ICOMOS Slovenia, Ljubljana, pp 82–99
22. Douet J (2018) The Water Industry as World Heritage – Thematic Study. In: The international committee for the conservation of the industrial heritage (TICCIH)
23. Cercleux A-L, Merciu F-C, Peptenatu D (2014) Conversion of Water towers-an instrument for conserving heritage assets. Urbanism Arhitectura Constructii 5:3
24. Dutta S, Jain S, Murty C (2001) Inelastic seismic torsional behaviour of elevated tanks. J Sound Vib 242:151–167
25. Mohammad Mansour A, Kassem MM, Mohamed Nazri F (2021) Seismic vulnerability assessment of elevated water tanks with variable staging pattern incorporating the fluid-structure interaction. Structures 34:61–77. https://doi.org/10.1016/j.istruc.2021.07.062
26. Mori C, Sorace S, Terenzi G (2015) Seismic assessment and retrofit of two heritage-listed R/C elevated water storage tanks. Soil Dyn Earthq Eng 77:123–136. https://doi.org/10.1016/j.soildyn.2015.05.007
27. Soroushnia S, Tafreshi ShT, Omidinasab F et al (2011) Seismic performance of RC elevated water tanks with frame staging and exhibition damage pattern. Procedia Eng 14:3076–3087. https://doi.org/10.1016/j.proeng.2011.07.387
28. Hirde S, Bajare A, Hedaoo M (2011) Seismic performance of elevated water tanks. Intl J Adv Engr Res Stud 1(1):78–87
29. Dutta SC, Jain SK, Murty CVR (2000) Alternate tank staging configurations with reduced torsional vulnerability. Soil Dyn Earthq Eng 19(3):199–215. https://doi.org/10.1016/S0267-7261(00)00004-X.
30. Shenton HW, Hampton FP (1999) Seismic response of isolated elevated water tanks. J Struct Eng 125:965–976. https://doi.org/10.1061/(ASCE)0733-9445(1999)125:9(965)
31. Martelli A, Forni M, Clemente P Recent Worldwide Application of Seismic Isolation and Energy Dissipation and Conditions for Their Correct Use
32. Drosos JC, Tsinopoulos SV, Karabalis DL (2005) Seismic response of spherical liquid storage tanks with a dissipative bracing system. In: 5th GRACM International congress on computational mechanics, Limassol. pp 313–319
33. Summers P, Castellano M, Bergamo G, et al (2008) Seismic risk reduction at petrochemical and LNG facilities: main results from INDEPTH project. In: Proceedings of the 14th world conference on earthquake engineering. Beijing, China. pp 06–0069
34. Nayak CB, Thakare SB (2019) Seismic performance of existing water tank after condition ranking using non-destructive testing. Int J Adv Struct Eng 11:395–410. https://doi.org/10.1007/s40091-019-00241-x
35. Guarnieri A, Milan N, Vettore A (2013) Monitoring Of complex structure for structural control using terrestrial laser scanning (Tls) and photogrammetry. Int J Archit Herit 7:54–67. https://doi.org/10.1080/15583058.2011.606595
36. Fabris M, Fontana Granotto P, Monego M (2023) Expeditious low-cost SfM Photogrammetry and a TLS survey for the structural analysis of illasi castle (Italy). Drones 7:101. https://doi.org/10.3390/drones7020101
37. Felice G, Choueri C, Meriggi P, Yanez Chura R (2023) An integrated approach for the investigation of the seismic behaviour of churches: the case study of St. Maria Maggiore in Tuscania, Procedia Structural Integr 44:2122–2127. https://doi.org/10.1016/j.prostr.2023.01.271.
38. Manual AMU (2022) Professional Edition, Version 1.8. Agisoft LLC
39. Dutta SC, Jain SK, Murty CVR (2001) Inelastic seismic torsional behaviour of elevated tanks. J Sound Vib 242:151–167. https://doi.org/10.1006/jsvi.2000.3343
40. UNI 9916:2004 – 01-04-2004 - Criteri di misura e valutazione degli effetti delle vibrazioni sugli edifici
41. (2016) DIN 4150-3:2016-12 Erschütterungen im Bauwesen – Teil 3: Einwirkungen auf bauliche Anlagen (Vibrations in buildings – Part 3: Effects on structures)
42. Yuanjun H, Yinfeng D, Feiyu G, Yutong L (2021) Structure modal identification based on computer vision technology. Vib Procedia. 37:72–77. https://doi.org/10.21595/vp.2021.21945
43. Konstantinidis D, Stathaki T, Argyriou V (2019) Phase amplified correlation for improved sub-pixel motion estimation. IEEE Trans Image Process 28:3089–3101
44. Śmieja M, Mamala J, Prażnowski K et al (2021) Motion magnification of vibration image in estimation of technical object condition-review. Sensors 21:6572. https://doi.org/10.3390/s21196572
45. Fioriti V, Roselli I, Cataldo A et al (2022) Motion magnification applications for the protection of Italian cultural heritage assets. Sensors 22:9988. https://doi.org/10.3390/s22249988
46. Valente NA, Do Cabo CT, Mao Z, Niezrecki C (2022) Quantification of phase-based magnified motion using image enhancement and optical flow techniques. Measurement 189:110508. https://doi.org/10.1016/j.measurement.2021.110508
47. Duan D-Y, Kuang KSC, Wang Z-C, Sun X-T (2023) Video motion magnification and subpixel edge detection-based full-field dynamic displacement measurement. Struct Control Health Monit 2023:e7904198. https://doi.org/10.1155/2023/7904198
48. Civera M, Zanotti Fragonara L, Surace C (2020) An experimental study of the feasibility of phase-based video magnification for damage detection and localisation in operational deflection shapes. Strain 56:e12336. https://doi.org/10.1111/str.12336
49. Wu H-Y, Rubinstein M, Shih E, et al (2012) Eulerian video magnification for revealing subtle changes in the world. ACM Transactions on Graphics (Proceedings of SIGGRAPH 31:
50. Chen JG, Wadhwa N, Cha YJ et al (2015) Modal identification of simple structures with high-speed video using motion magnification. J Sound Vib 345:58–71
51. Wadhwa N, Wu H-Y, Davis A et al (2016) Eulerian video magnification and analysis. Commun ACM 60:87–95. https://doi.org/10.1145/3015573
52. Chen JG, Davis A, Wadhwa N et al (2017) Video camera-based vibration measurement for civil infrastructure applications. J Infrastruct Syst 23:B4016013. https://doi.org/10.1061/(ASCE)IS.1943-555X.0000348
53. Tomasi C, Kanade T (1991) Detection and tracking of point. Int J Comput Vis 9:3
54. Harris FJ (1978) On the use of windows for harmonic analysis with the discrete fourier transform. Proc IEEE 66:51–83. https://doi.org/10.1109/PROC.1978.10837

55. Oppenheim AV (1999) Discrete-time signal processing. Pearson Education India
56. Proakis JG (2007) Digital signal processing: principles, algorithms, and applications, 4/E. Pearson Education India
57. Bendat JS, Piersol AG (2000) Random data analysis and measurement procedures. Meas Sci Technol 11:1825–1826
58. Sangirardi M, Altomare V, de Felice G (2024) Computer-vision based structural health monitoring: novel techniques for modal identification (in preparation).
59. Smith LI (2002) A tutorial on principal components analysis
60. Oprsal I, Eisner L (2014) Cross-correlation—an objective tool to indicate induced seismicity. Geophys J Int 196:1536–1543. https://doi.org/10.1093/gji/ggt501
61. Jackson JE (2005) A user's guide to principal components. John Wiley & Sons
62. Jolliffe IT (2002) Principal component analysis for special types of data. Principal component analysis. Springer, New York, NY, pp 338–372